Cytokine 62 (2013) 217–225

Contents lists available at SciVerse ScienceDirect

Cytokine

journal homepage: www.journals.elsevier.com/cytokine

TNF-alpha and melphalan modulate a specific group of early expressed genes in a murine melanoma model

Vladmir Cláudio Cordeiro de Lima [a,b,*], Alex Fiorini de Carvalho [c], Mariana Morato-Marques [a], Vivian Lika Hashimoto [a], Graziela Machado Gruner Turco Spilborghs [a], Sarah Martins Marques [g], Gilles Landman [d], Cesar Torres [e], Karina Braga Ribeiro [f], Helena Brentani [e], Luiz F.L. Reis [g], Adriana Abalen Martins Dias [h]

[a] Laboratório de Inflamação e Câncer, Fundação Antônio Prudente, Hospital AC Camargo, São Paulo, Brazil
[b] Departamento de Oncologia Clínica, Fundação Antônio Prudente, Hospital AC Camargo, São Paulo, Brazil
[c] Laboratório de Genômica Funcional, Fundação Antônio Prudente, Hospital AC Camargo, São Paulo, Brazil
[d] Departamento de Anatomia Patológica, Fundação Antônio Prudente, Hospital AC Camargo, São Paulo, Brazil
[e] Laboratório de Bioinformática, Fundação Antônio Prudente, Hospital AC Camargo, São Paulo, Brazil
[f] Departamento de Epidemiologia, Faculdade de Medicina da Santa Casa de Misericórdia de São Paulo, São Paulo, Brazil
[g] Hospital Sírio-Libanês, São Paulo, Brazil
[h] Laboratório de Genética Experimental, Departamento de Biologia Geral, Instituto de Ciências Biológicas, Universidade Federal de Minas Gerais, Belo Horizonte, Minas Gerais, Brazil

ARTICLE INFO

Article history:
Received 22 February 2012
Received in revised form 21 January 2013
Accepted 11 February 2013
Available online 25 March 2013

Keywords:
Melphalan
TNF-alpha
Melanoma
Microarray
Early expression genes

ABSTRACT

Background: Cutaneous melanoma displays high morbidity and mortality rates. Isolated limb perfusion with melphalan (Mel) is used for the treatment of non-resectable, locally advanced extremity melanomas. When combined with tumor necrosis factor alpha (TNF-alpha) treatment, the complete response varies between 70% and 90%. The mechanisms underlying the effects of Mel and TNF-alpha are not completely understood. We evaluated the impact of systemic Mel and TNF-alpha administration on tumor growth, analyzed the morphological changes promoted by each treatment, and identified early expressed genes in response to Mel and TNF-alpha treatment, either alone or in combination, in a murine melanoma model.

Methods: Six- to eight-week-old male mice were subcutaneously inoculated with B16F10 melanoma cells and then intravenously injected with TNF-alpha, melphalan or a combination of both drugs when the tumors reached 1.0 cm^2. Tumor growth was monitored every other day, and histological analysis was performed when the tumors reached 3.0 cm^2. Total RNA was extracted from the resected tumors and submitted to amplification, labeling and hybridization on an oligonucleotide microarray (Fox Chase Cancer Center). Tumor growth and histological parameters were compared using ANOVA. Survival curves were calculated using the Kaplan–Meier method. Two-way ANOVA was used to identify differentially expressed genes among the various treatments, and Dunn's test was used for pair-wise comparisons.

Results: Systemic administration of Mel impaired tumor growth ($p < 0.001$), improved animal survival ($p < 0.001$), and decreased mitotic rate ($p = 0.049$). Treatment with TNF-alpha alone had no impact, neither on tumor growth, nor on survival, but it increased necrosis ($p < 0.024$) and decreased mitotic rates ($p = 0.001$) in the tumors. Combined treatment with Mel and TNF-alpha had similar effects in tumor growth, survival, necrosis and mitotic rate as observed with individual treatments. Moreover, 118 genes were found differentially expressed by microarray analysis and 10% of them were validated by RT- real time PCR. In our model we found that the treatments regulate genes that play important roles in tumorigenesis such as cell adhesion (*Pard3*, *Pecam1*, *Ilk*, and *Dlg5*), proliferation (*Tcfe3* and *Polr1e*), cell motility (*Kifap3*, *Palld*, and *Arhgef6*), apoptosis (*Bcl2l11*), and angiogenesis (*Flt1*and *Ptprj*).

Conclusions: Our data reproduces, in mice, some of the features observed in melanoma patients treated with the combination of Mel and TNF-alpha. The identification of genes with altered expression by these drugs both individually and in combination might help in the understanding of their mechanism of action and, as a consequence, improved strategies that could impact their clinical application.

1. Introduction

Cutaneous melanomas are malignant, radio- and chemoresistant neoplasias that originate from melanocytes. Although

* Corresponding author. Address: R. Prof. Antônio Prudente, 211 Hospital AC Camargo, Departamento de Oncologia Clínica, 01509-900 São Paulo, SP, Brazil. Tel.: +55 11 2189 5000; fax: +55 11 2189 5108.
E-mail address: vladmirlima@yahoo.com.br (V.C.C. de Lima).

1043-4666
http://dx.doi.org/10.1016/j.cyto.2013.02.022

melanomas correspond to only 4% of all skin cancers, they present high morbidity and elevated mortality rates (80%) [1]. Melanomas are the most common tumor among young women, the seventh most common cancer among women in general, and the fifth most common tumor among men [2]. It has been estimated that 62,480 new cases of melanoma occurred in the USA alone in 2009, of which 8440 represented lethal cases. Surgical excision is the treatment of choice for this type of tumor; it is associated with a 10-year survival rate of 89% for stage IB tumors and a 5-year survival rate of 40% for stage IIIC tumors [3]. Adjuvant treatment with interferon-gamma reduces recurrence rates but has no significant impact on survival [4]. Two-thirds of patients with metastatic disease display loco-regional spreading, including satellitosis and in-transit metastasis, which includes 21% of all metastatic cases. Amputation is the first choice treatment for in-transit metastasis and unresectable, locally advanced melanoma, with long-lasting control rates of 21–33% [5]. As an alternative treatment, isolated limb perfusion (ILP) is a less morbid option that causes no mutilation [6], especially in the case of bulky ($\geqslant$3.0 cm) or multiple lesions ($\geqslant$15 lesions) [7]. In this approach, melphalan (Mel), a bifunctional alkylating agent that induces apoptosis [8], is the drug of choice, resulting in complete response rates of 40–50% [9,10]. Although melphalan is frequently used in the treatment of multiple myeloma, the systemic use of Mel in melanoma therapy is not possible because the required doses are highly toxic. The efficacy of the ILP procedure relies on high intratumoral Mel concentrations (20-fold higher than the systemic doses).

The combination of TNF-alpha and Mel increases complete response rates to up 90%, limb salvage rates to 84% [7,9–11] and 5-year overall survival rates to 42%. These results are very similar to those associated with surgical management (25–30%) [7].

Two randomized phase III trials evaluated the role of ILP in advanced-stage limb melanomas. Fraker et al. (2002) (unpublished data) have shown an increase in complete response rates, notably in larger tumors (58% vs. 19% in smaller tumors), for the TNF-alpha plus melphalan arm of the trial. The other trial was negative for primary end-points but presented a non-statistically significant improvement in complete response rates after 6 months for the combination arm of the study. A larger number of patients who displayed a complete response to TNF-alpha plus melphalan after 3 months maintained that response for 6 months in the combination arm of the study [5].

The most accepted mechanism for this synergistic effect is that TNF-alpha promotes the detachment of the endothelial cells of tumor vessels from the basal membrane, thereby increasing vascular permeability, which in turn facilitates the penetration and intratumoral accumulation of Mel [12,13]. The alterations in the tumors promoted by TNF-alpha also prompt tumoral vasculature to undergo erythrostasis, leukostasis, and intravascular coagulation, which impair the afflux of nutrients and oxygen. This creates an environment that is more susceptible (low pH) to Mel activity, which leads to tumor hemorrhagic necrosis [14–16]. Apart from this suggested mechanism regarding the combination of TNF-alpha and Mel, the cellular and molecular mechanisms underlying the alterations promoted by these two molecules are not completely understood.

The use of Mel and TNF-alpha in combination in ILP suggests that the identification of the molecular targets triggered by the combination of these two drugs may reveal putative pharmacologic targets for the systemic treatment of melanomas using lower doses of melphalan in combination with alternative agents that are less toxic than TNF-alpha.

In this study, we evaluated the impact of systemic Mel and TNF-alpha administration on tumor growth, analyzed the morphological changes promoted by each treatment, and identified the early molecular targets of Mel and TNF-alpha, either alone or in combination, in a murine melanoma model.

2. Material and methods

2.1. Animals

For all experiments, male C57BL/6 mice (9–10 animals per group, as indicated) of 6–8 weeks of age were used. The mice were maintained in individually ventilated cages housed in a clean, temperature-controlled room with a 12 h light/12 h dark cycle with access to sterilized food and water *ad libitum*. All procedures that involved animal experimentation were approved by the Institutional Animal Care and Use Committee (animal ethics license number 016/07) and were in accordance with the International Ethical Guidelines.

2.2. Cells

B16F1 and B16F10 mouse melanoma cells were kindly provided by the Ludwig Institute for Cancer Research (São Paulo, Brazil) and by Dr. Ronaldo Travassos (São Paulo Federal University – São Paulo, Brazil), respectively. The cell lines were maintained in RPMI medium (Gibco BRL) supplemented with 10% fetal calf serum (Cultilab), 2.0 mM L-glutamine (Sigma), and 40 μg/ml gentamicin (Schering-Plough) at 37 °C and 5% CO_2. Sub-confluent cultured cells (up to four passages only) were detached with 0.02% trypsin, harvested in complete medium, washed and resuspended in PBS. Cell viability was assessed via Trypan blue assay, and only cultures with $\geqslant$90% viable cells were used for the experimental induction of tumors in mice. The melanoma cell lines K1735M2 and M2R, which were used in the preparation of the reference RNA, were a kind gift from Dr. Jan Vilcek (New York University Medical Center) and Dr. Shigeko Sonehara (University of São Paulo) and were maintained in DMEM under the same conditions described above.

2.3. In vivo model

For tumor implantation, mice were manually restrained and 5.0×10^5 melanoma cells (in 100 μL PBS) were subcutaneously injected in both rear flanks. Tumor growth was evaluated every 2 days by direct measurement with a caliper, and tumor size was calculated as the product of the two greatest perpendicular diameters. Mice bearing tumors of 1.0 ± 0.3 cm^2 ($\sim$10 days after tumor implantation) were randomly assigned to be intravenously injected with 100 μL of one of the following treatments: (i) Mel (n = 10), 12.0 mg/kg melphalan (Alkeran, Glaxo-Smith-Kline); (ii) TNF-alpha (n = 10), 0.05 mg/kg recombinant murine TNF-alpha (R&D); and (iii) Mel + TNF-alpha (n = 9), the combination of the two agents at the aforementioned doses. Control mice (n = 10) were injected intravenously with 100 μL saline. The selected doses displayed no systemic toxicity when previously evaluated *in vivo* (data not shown). Three hours after treatment, the animals were anesthetized with ketamine (Vetanarcol, König)/thiazine (Rompun, Bayer) (60.0/15.0 mg/kg i.p.), and the tumors implanted on the left flank were surgically removed. One portion of the harvested tumor was snap-frozen in liquid nitrogen for posterior RNA extraction, and the other portion was fixed in 10% phosphate-buffered formalin (PBF) for histological analysis. The growth of the remaining right-flank tumors was monitored every 2 days to assess the efficacy of each treatment. The mice were sacrificed when the tumors reached 3.0 cm^2 to avoid animal suffering.

2.4. Histological analysis

Tumor sections (5.0 μm thick) removed from the left flanks and fixed in PBF were stained with hematoxylin–eosin. Digitalized images were obtained using an optical microscope (Axioscope 40,

Zeiss) connected to a digital camera (MPEG Movie EX, Sony). For each tumor slide, 10 non-overlapping random fields were photographed at high magnification (400×). Images were blindly analyzed using AxioVision software (version 3.1, Zeiss) by a single experienced pathologist. The following parameters were considered: total tumor area, total melanoma cell count, and percentage of necrotic, hemorrhagic, and mitotic cells. Vascular density was assessed after immunostaining for CD34 (SC7045, 1:100, Santa Cruz) using a 270 × 270 μm grid. For each sample, 20 non-overlapping random fields were examined and every tubular structure with a clearly defined lumen, which was lined with plain cells on the reticulum grid, was counted (vascular structures were classified as either CD34+ or CD34−). The tumor area was estimated by multiplying the percentage of the grid area occupied by the tumor and the total area of the grid.

2.5. RNA extraction, purification, and amplification

Total RNA was isolated using Trizol reagent (Invitrogen, USA) and a tissue disruptor (Polytron, Kinematika, Germany). After disruption, the sample was spun at 12,000*g* and 4 °C to remove melanin. The RNA in the remaining clear pink suspension was then extracted as recommended by the manufacturer. Total RNA was purified using a RNeasy Midi Kit (Qiagen) following the manufacturer's recommendations, reverse-transcribed using ImProm-II™ RT (Promega) and oligo-dT (24)-T7 primers, and submitted to two rounds of amplification using a RiboMax kit (Promega) following the protocol proposed by Gomes et al. [17].

2.6. Microarray gene expression analysis

We used amplified RNA (aRNA) isolated from 18 tumor samples (Control – 5 samples; Mel – 4 samples; TNF-alpha – 4 samples; and Mel + TNF-alpha – 5 samples) in the gene expression analysis by microarray. For replica hybridization with dye swap, aRNA isolated from both the tumors and a pool composed of equal amounts of RNA extracted from the K1735M2, M2R, B16F10, and B16F1 melanoma cells were labeled with either Alexa Fluor 555 or Alexa Fluor 647. The labeled aRNA samples were hybridized against a glass platform containing 16,128 immobilized sense oligonucleotides (Fox Chase Cancer Center, USA) corresponding to murine genes. The pre-hybridization, hybridization, and washing conditions are detailed in the online data Supplement. The slides were scanned with a confocal laser scanner (ScanArrayTM Express, Perkin–Elmer Life Sciences, USA) with a 10 μm resolution and a PMT of 60% for Alexa Fluor555 and 70% for Alexa Fluor 647, and the data were extracted with ScanArray Express software (Packard BioScience) using the histogram method. Each slide generated a data set for each channel corresponding to the Alexa Fluor 555 and Alexa Fluor 647 dyes. The locally weighted scatter-plot smoothing method (LOWESS), which was adjusted for linear and non-linear systematic variations, both of the intensity-dependent types, and primarily for low intensity spots, was employed for data normalization. The complete array data set was deposited at NCBI Gene Expression Omnibus (GEO, http://www.ncbi.nlm.nih.gov/geo/) under series number GSE21559. The Pearson's correlation coefficient was used to determine the reproducibility of the experiment in which duplicate hybridizations were performed (main and dye swap), and the data are represented on a dispersion graph (MM plot). A two-way ANOVA was used to identify the differentially expressed genes among the various treatments, while Tukey's test was used for pairwise comparisons. The comparisons were considered statistically significant when $p \leqslant 0.05$. *P* values adjusted for multiple comparisons (*q* value) were also calculated, assuming a false discovery rate (FDR) of 10%. The genes displaying a relative gene expression (fold) greater or equal to 1.5 were investigated further. For these analyses, the TM4-Microarray Software Suite [18] and the R package were employed.

2.7. Reverse transcription and real time PCR

Two-thirds of the samples employed in the real time PCR assays were derived from a different set of tumor samples than those used in the microarray, and the other one-third of the samples was derived from the same set that was used in the microarray (Control – 3 samples; Mel – 5 samples; TNF-alpha – 5 samples; and Mel + TNF-alpha – 5 samples). Two micrograms of total RNA were reverse-transcribed using ImProm-II™ RT reverse transcriptase (Promega, USA) and oligo dT-primers according to the manufacturer's instructions. Specific primer sequences and detailed quantitative real time PCR conditions are available in the online data Supplement. A pool of RNAs obtained from the saline-injected control mice was used as reference, and the relative expression ratio was calculated in accordance with the protocol provided by Pfaffl [19]. The housekeeping gene hypoxanthine–guanine phosphoribosyl-transferase (*Hprt*) was used for normalization.

2.8. Statistical analysis

Tumor growth was compared among the groups and time points using repeated measures ANOVA followed by a *post hoc* Tukey-HSD test. ANOVA followed by Tukey's test were employed to compare the mean values of the photographed total tumor area, total melanoma cell count, necrosis to total tumor area ratio, hemorrhage to total tumor area ratio, and mitosis to total cell count ratio. The mean values for the hemorrhage to total area ratio were compared using the Kruskal–Wallis test followed by Tukey's test. The real time PCR data were compared via ANOVA followed by Tukey's test or a Kruskal–Wallis test followed by a Mann–Whitney test, as appropriate. Progression-free survival curves (the time required for the tumors to reach 3.0 cm^2) were calculated using the Kaplan–Meier method. The curves were compared using a log-rank test followed by the Cox regression method. A two-way ANOVA was used to identify the differentially expressed genes among the various treatments, while the Dunn test was used for pairwise comparisons. The statistical packages Statistica 5.0 and SPSS for Windows (version 15.0) were employed for these analyses. Results were deemed statistically significant when $p < 0.05$.

3. Results

3.1. Impact of systemic Mel and TNF-alpha administration on tumor growth

Three hours after the treatment, the tumors of the left flank were surgically removed, and the growth of the remaining tumor (right flank) was monitored until it reached 3.0 cm^2. As shown in the upper panel of Fig. 1, in mice treated with saline or TNF-alpha alone, a significant increase in tumor size was observed between D0 (day of treatment initiation) and D6 (6 days after treatment initiation) ($p = 0.0001$ for both). However, the systemic administration of Mel promoted a delay in tumor growth, and no significant augmentation in the size of the tumors was observed between D0 and D6 in the groups treated with Mel alone ($p = 0.052$) or Mel + TNF-alpha ($p = 0.215$). At D6, the tumors derived from mice treated with Mel or Mel + TNF-alpha were significantly smaller than their saline- or TNF-alpha-injected counterparts ($p < 0.001$). The addition of TNF-alpha at the dose adopted in this study did not improve the effect of Mel on tumor growth ($p = 0.296$ for Mel vs. Mel + TNF-alpha), and the significant difference in the size of the tumors in the Mel + TNF-alpha mice compared with the

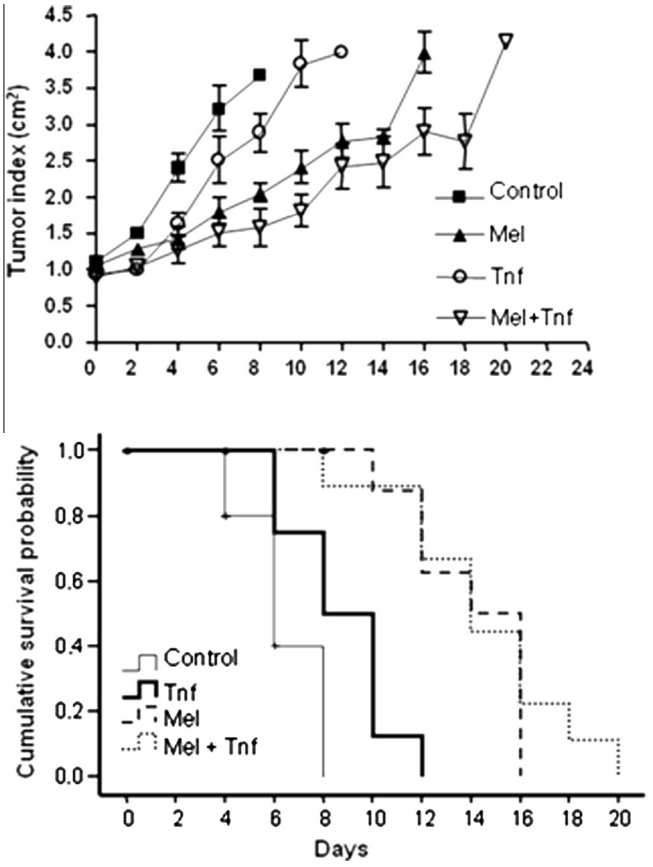

Fig. 1. Impact of treatment with melphalan and Tnfa on melanoma tumor growth and progression-free survival in mice. Mice bearing tumors of 1.0 ± 0.3 cm^2 were treated intravenously with saline (control group, $n = 10$), Tnfa ($n = 10$), melphalan ($n = 10$), or with associated treatment (Mel + Tnf, $n = 9$). Upper panel: results are shown as the mean and SEM of the tumor index obtained from the product of the two largest perpendicular transversal diameters of the tumors (tumor index). Comparisons were done by ANOVA followed by Tukey's test. Lower panel: Curves were calculated by Kaplan–Meier method and comparisons were done by log-rank test, followed by Cox-Regression. Mel + Tnf x Control HR = 0.034 95%CI 0.008–0.215, $p < 0.001$. Mel × Control HR = 0.041 95%CI 0.006–0.18, $p < 0.001$. Tnf × Control HR = 0.28 95%CI 0.073–1.10, $p = 0.069$.

TNF-alpha-treated mice depicts the preponderant activity of Mel ($p = 0.006$). No differences in the size of the tumors at D6 were observed between the control and TNF-alpha groups ($p = 0.296$). We observed a reduced rate of tumor growth when comparing the Mel group with the TNF-alpha group (Mel vs. TNF-alpha, $p = 0.10$).

As shown in the lower panel of Fig. 1, the delay in tumor growth promoted by Mel impacted the progression-free survival (PFS) of the Mel-treated mice. This delay was higher and statistically significant compared with the controls, both in mice treated with Mel (HR = 0.041 95%CI 0.006–0.18, $p < 0.001$) and in those treated with Mel + TNF-alpha (HR = 0.034 95%CI 0.008–0.215, $p < 0.001$). Nevertheless, there was no difference between the control and TNF-alpha groups ($p = 0.069$), and no improvement in survival was observed when TNF-alpha was combined with Mel ($p = 0.821$ for the Mel and Mel + TNF-alpha groups).

The same treatment response was observed in mice bearing B16F1-implanted tumors (see online data Supplement, Figs. 1 and 2).

3.2. Morphological changes promoted by the Mel and TNF-alpha treatments

The photomicrographs displayed in Fig. 2 shows the main alterations in morphology observed in the tumors 3 h after treatment with Mel and TNF-alpha, as described earlier. In all groups that received Mel and/or TNF-alpha, we observed a decrease in the total number of mitotic cells compared with the control saline-treated group (Table 1 and online Supplementary data Fig. 3). Increased levels of necrosis were observed in the groups treated with TNF-alpha alone ($p = 0.017$) or in combination with Mel ($p = 0.015$) compared with the control group (Table 1 and Fig. 2). No difference was observed between the groups treated with TNF-alpha alone and Mel + TNF-alpha ($p = 0.233$).

Three hours after treatment, no modification in vascular density was observed in response to any treatment (online Supplementary data Table 1).

3.3. Microarray gene expression profiling

A total of 596 elements that were differentially expressed among treatments were identified via ANOVA. Due to oligonucleotide redundancy, these 596 elements corresponded to 118 genes (a complete list is provided in the online data Supplement Tables 2 and 3). These 118 genes were used to create the non-supervised hierarchical cluster shown in Fig. 3. In the image, color intensity is proportional to the log2 of the sample to reference intensity ratio and varies from −3 to +3. The samples that received the same treatment grouped together almost perfectly, according to this set of genes. Using SOM (self organizing maps) analysis, it was possible to identify subgroups of genes that displayed similar patterns of expression in response to each treatment (online data Supplement Table 4).

Real time PCR was used to validate the expression of 11 candidate early targets that were differentially expressed according to the microarray analysis and showed relative expression rates of at least $\geqslant 1.5$. The candidates were arbitrarily selected to match 10% of all differentially expressed genes. These genes included *Pard3*, *Dlg5*, *Arhgef6*, *Flt1*, *Ifi202b*, *Cck*, *Ptprj*, *Pecam1*, *Irak1bp1*, *Palld*, and *Bcl2l11* (Fig. 4). Seven of these genes (*Pard3*, *Flt1*, *Ptprj*, *Dlg5*, *Irak1bp1*, *Ifi202b*, and *Cck*) were either up- or downregulated in the same manner as that observed with the microarray in at least one of the groups. Among the genes selected for validation, two were differentially expressed between Mel and Mel + TNF-alpha (*Palld* and *Bcl2l11*), and Mel and TNF-alpha (*Palld*) in the microarray analysis (Fig. 4). Although *Fabp4* was not identified as statistically differentially expressed as assessed via microarray, this gene displayed the highest value of relative expression and a tendency to be downregulated in the groups treated with TNF-alpha (online data Supplement Fig. 4a). For this reason, *Fabp4* expression was also evaluated via real time PCR, and this trend was confirmed.

4. Discussion

The concomitant administration of TNF-alpha and Mel in the treatment of locally advanced extremity melanoma increases the response rate and eventually extends the tumor control time (Deroose et al. 2011). A recent meta-analysis of twenty-two studies of ILP for the treatment of melanoma demonstrated that ILP is a rather safe strategy with an acceptable overall survival (36.5% in 5 years) [20]. Nevertheless, the mechanisms underlying its effects are not clear. To identify potential molecular targets that may allow us to better understand the mechanisms involved in the interaction of Mel and TNF-alpha in melanoma treatment, we studied the gene expression profile of murine melanomas exposed to these therapeutic agents. Our study revealed many interesting potential targets for the development of therapeutic strategies that may be used in the future to improve ILP results and for the systemic use of alkylating drugs, such as melphalan, in combination with alternative agents that are less toxic than TNF-alpha.

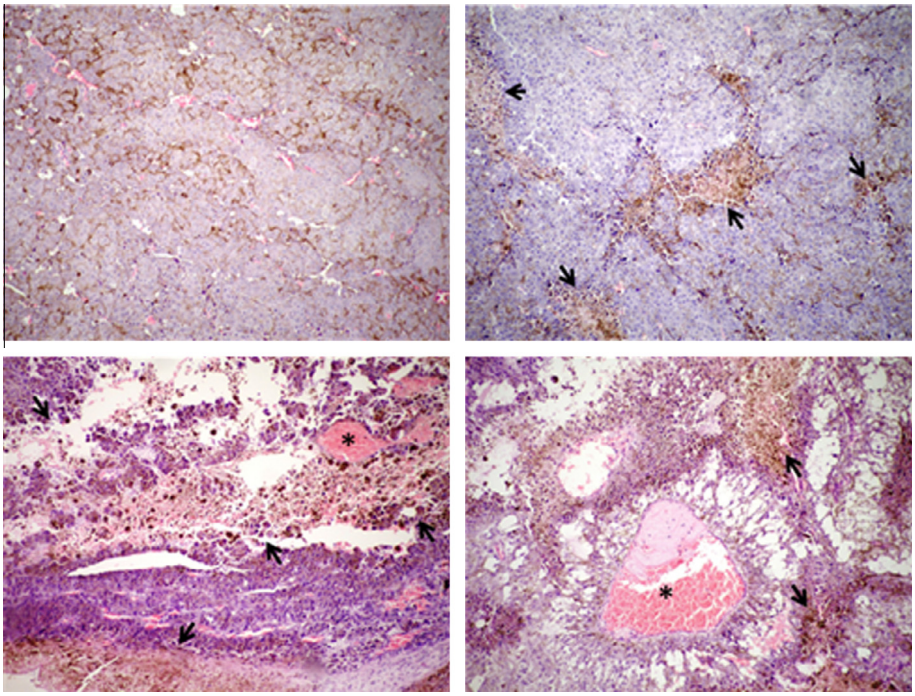

Fig. 2. Representative microphotographs of hematoxylin–eosin stained major histological changes observed 3 h after treating melanoma with melphalan and Tnfa in mice. Left upper panel: Control group (saline-treated animals). Tumor tissue architecture is preserved with no necrosis or hemorrhage area. Right upper panel: Although necrotic areas are observed in Melphalan-treated animals, the tissue architecture is preserved. Left lower panel: extensive necrotic areas (arrows) and dilated blood vessels with thrombus in their lumen (*) are observed in the tumors extracted from Tnfa-treated animals. Right lower panel: extensive necrosis (arrows) associated with blood vessel dilation, luminal thrombuses (*), and impressive intercellular edema are presented in the tumors collected from mice treated with Mel + Tnf. All pictures were taken under magnification of 100×.

Although TNF-alpha is classically described as a promoter of extensive hemorrhagic necrosis in tumors [21], in our study, TNF-alpha did not promote significant differences in hemorrhage or vascular density, which was most likely due to the short drug exposure time prior to tumor removal. Despite this observation, the efficacy of our different treatment regimens is reflected in the impairment of tumor growth, the promotion of necrosis, and detectable changes in the gene expression profile of the tumors. The isolated treatment with Mel led to a delay in tumor growth and a decrease in the mitotic index. The primary effect observed by the addition of TNF-alpha was the increase in tumor necrosis.

Although TNF-alpha alone also reduced the mitotic rate and promoted massive tumor necrosis, these effects did not represent significant tumor growth arrest or better progression-free survival, which was most likely due to the rapid proliferation of tumor cell remnants in the periphery of the necrotic areas. We and others [21] have observed that *in vitro*, TNF-alpha does not exert a direct cytotoxic or cytostatic effect on B16F10 or B16F1 cells (data not shown). In contrast, Mel was shown to be cytotoxic to B16F10 cells and inhibit tumor growth.

We identified a set of 118 genes that responded to systemic treatment with Mel and TNF-alpha; we hypothesize that some of these genes play important roles in tumorigenesis and the mediation of antitumoral effects, such as cell adhesion (*Pard3*, *Pecam1*, *Ilk*, and *Dlg5*), proliferation (*Tcfe3* and *Polr1e*), cell motility (*Kifap3*, *Palld*, and *Arhgef6*), apoptosis (*Bcl2l11*), and angiogenesis (*Flt1*and *Ptprj*), which could be targeted for drug development. A non-supervised hierarchical cluster based on these 118 differentially expressed genes (Fig. 3) allowed us to sort the various treatment groups almost perfectly. The combination of Mel and TNF-alpha modulated the expression of 59 genes. By comparing our *in vivo* and *in vitro* data sets, we hypothesize that the primary targets of Mel activity are most likely the melanoma cells themselves, while TNF-alpha seems to act preferentially on cells in the tumor micro-environment, as B16F10 cells receiving the same treatment *in vitro* did not display the gene modulation observed in the *in vivo* model (online data Supplement Fig. 5).

We centered our discussion on six (*Arhgef6*, *Ifi202b*, *Igf2bp3*, *Pard3*, *Flt1*, and *Cck* (Table 2)) of the 11 genes that displayed a p value $\geqslant 0.05$ and a relative expression (fold) $\geqslant 1.5$.

The *Arhgef6* gene (Rac/Cdc42 guanine nucleotide exchange factor 6) (Table 2 and online Supplementary data Table 3) was downregulated by treatment with TNF-alpha alone or in combination with Mel. Our data and that reported by others [22–25] support the idea that reduced ARHGEF6 levels may lead to increased vascular permeability, endothelial cell detachment and enhanced

Table 1
Histopathological parameters compared among mice treated intravenously with saline (control), melphalan (Mel), TNF-alpha (TNF-alpha), or a combination of both drugs (Mel + TNF-alpha). All comparisons were performed in relation to the control group. An ANOVA or Kruskal–Wallis test followed by Tukey's test was employed for multiple comparisons among groups, and the results were considered statistically significant when $p < 0.05$ (*). The results are expressed as the mean ± SEM.

Groups	Analyzed tumor area ($\times 10^3$ μm^2)	Total melanoma cell count	Mitosis (%)	Necrosis (%)	Hemorrhage (%)
Control	33.88 ± 3.86	78.6 ± 7.09	0.7 ± 0.15	8.2 ± 5.3	0.7 ± 0.51
Mel	33.1 ± 5.54	71.0 ± 5.43	0.33 ± 0.16*	18.22 ± 3.15	1.0 ± 0.6
Tnf	33.5 ± 2.34	57.5 ± 8.51	0.1 ± 0.1*	33.1 ± 7.21*	4.7 ± 2.91
Mel + Tnf	32.89 ± 6.83	52.66 ± 5.32	0.22 ± 0.14*	34.56 ± 6.43*	2.44 ± 1.63

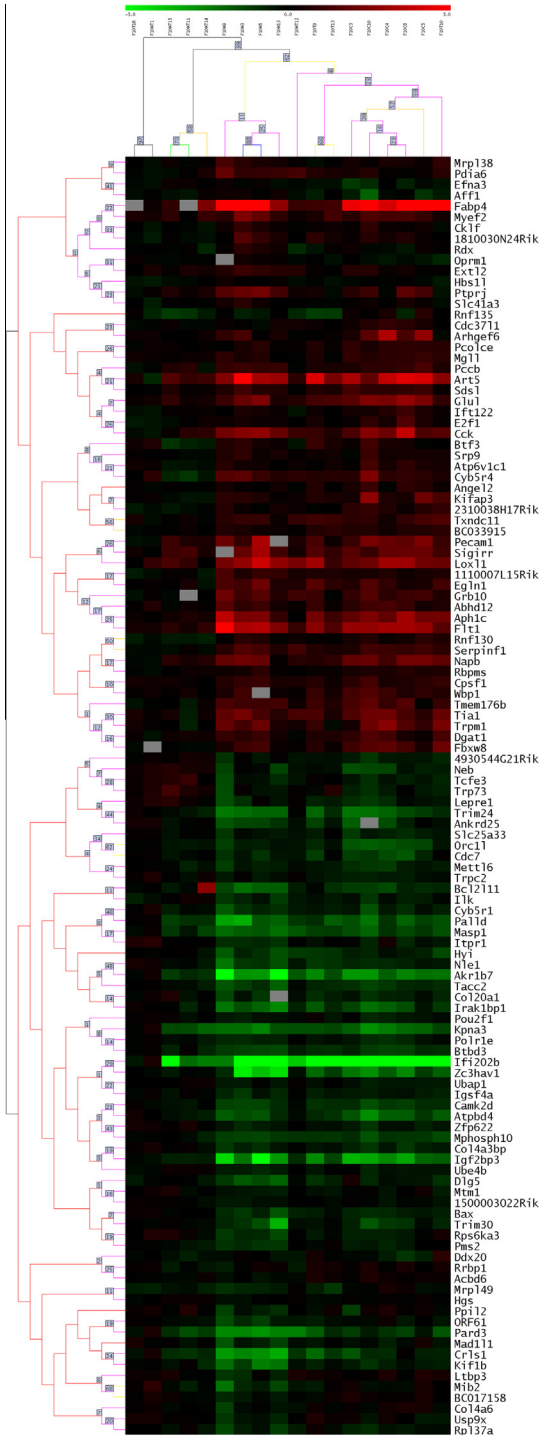

Fig. 3. Non-supervised hierarchical clustering based on differentially expressed genes as a function of the type of treatment. Samples were grouped according to correlation distances among the 118 genes identified by ANOVA using a Pearson's linear correlation test. Color intensity correlates with the sample to reference signal intensity ratio. In green are those genes in which expression was down-regulated by the treatment, and in red are those in which the expression was up-modulated. Missed data are represented by grey boxes; sample identification is on the top. On the right are the gene symbols of the elements used to build the cluster. Samples: tumors of 1.0 ± 0.3 cm^2 recovered from C57BL/6 mice treated intravenously for 3 h with saline (C), Tnfa 0.05 mg/kg (T), melphalan 12 mg/kg (M), or both (MT). (For interpretation of the references to color in this figure legend, the reader is referred to the web version of this article.)

susceptibility of the endothelia to TNF-alpha-induced apoptosis. ARHGEF6 integrates multiproteic complexes that mediate the formation of integrin clusters during the initial phases of cell adhesion to the extracellular matrix (ECM) [23], the establishment of focal adhesion, thereby contributing to cell migration [26] and invasion capacities [24]. ARHGEF6 is a positive modulator of Rho-like monomeric G-proteins (Rac1 and Cdc42) [25], which mediate the activation of NFKB by TNF-alpha [22]. Inhibition of Cdc42 was shown to be associated with an elevation in caspase-3 activity and increased the susceptibility of HUVECs to apoptosis in response to TNF-alpha [27]. The downregulation of *Arhgef6* by TNF-alpha may play a role in PAK (p21-activated protein kinase) inhibition, which has been shown to exert activity against thyroid cancer cell lines [28].

Pard3 (partitioning defective 3 homolog) was one of the 20 genes modulated by Mel alone *in vivo*. The downregulation of *Pard3* could contribute to the increased endothelial permeability that favors the intratumoral accumulation of Mel. It is also possible that the low expression of *Pard3* could impair the ability of melanoma cells to correct the DNA damage induced by Mel, as PARD3 has been recently shown to modulate the activity of DNA-dependent protein kinase (DNA-PK) and PARD3 knockdown enhances irradiation susceptibility and promotes inadequate DNA break repair [29].

Upregulated by Mel and TNF-alpha, the protein encoded by *Ifi202b* (interferon activated gene 202B) inhibits NFKB and AP1 activity and sensitizes 3T3 cells to apoptosis when exposed to TNF-alpha [30]. IFI202B also inhibits cell proliferation and reduces tumorigenicity, invasiveness, metastatic potential, and angiogenesis [31]. As NFKB inhibition seems to be the primary mode of action of *Ifi202b*, drugs capable of promoting NFKB inactivation, such as bortezomib, should augment TNF-alpha efficacy or reproduce some of its effect on tumors, as suggested by recent reports [32].

Igf2bp3 (insulin growth factor binding-protein 3) encodes IMP3 (insulin-like growth factor II mRNA-binding protein 3), an oncofetal RNA-binding protein that is involved in cell growth and migration during the early stages of embryogenesis, cancer cell proliferation, and metastasis [33]. The expression of IMP3 correlates with melanoma progression and can help to differentiate nevi from malignant lesions [34,35]. *Igfbp3* levels were upregulated by Mel and TNF-alpha treatment in our model, with high relative gene expression ratios.

Cck (cholecystokinin) is an agonist of the gastrin and cholecystokinin receptors CCK-R1, CCK-R2, and CCK-R3. The inhibition of *Cck* expression in tumors, which was most likely mediated by TNF-alpha in our model, may be associated with tumor growth inhibition via a reduction of tumor cell motility and invasiveness or a blockade of tumor neo-angiogenesis. Various studies have shown that cholecystokinin promotes cell invasiveness, motility, and proliferation in melanomas, biliary duct and pancreatic cancer, and Ewing's tumor cell lines. Additionally, its suppression inhibits neo-angiogenesis in melanoma xenograft models [36–38].

The role of the vascular endothelial growth factor receptor-1 (FLT1/VEGFR1) in angiogenesis and hematopoiesis is not completely understood, but it is possible that it acts as a decoy receptor or a suppressor of signaling via vascular endothelial growth factor receptor-2 (KDR/VEGFR2) [39]. FLT1 may also induce macrophage migration and the recruitment of endothelial cell progenitors and may function as a strong positive regulator of angiogenesis during tumor growth [40]. *FLT1* encodes FLT1, which binds VEGFA, VEGFB, and PLGF (placental growth factor). The downregulation of *FLT1* in tumors exposed to TNF-alpha may be associated with reduced proliferative activity of the tumor endothelium and, in consequence, the inhibition of tumor growth. FLT1 has a ten-fold greater affinity for its ligands than KDR but significantly weaker tyrosine kinase activity. However, under pathologic conditions, in which PLGF expression is high, Flt1 may play an important role in neo-angiogenesis [41]. *FLT1* inhibition may also explain, at least in part, the

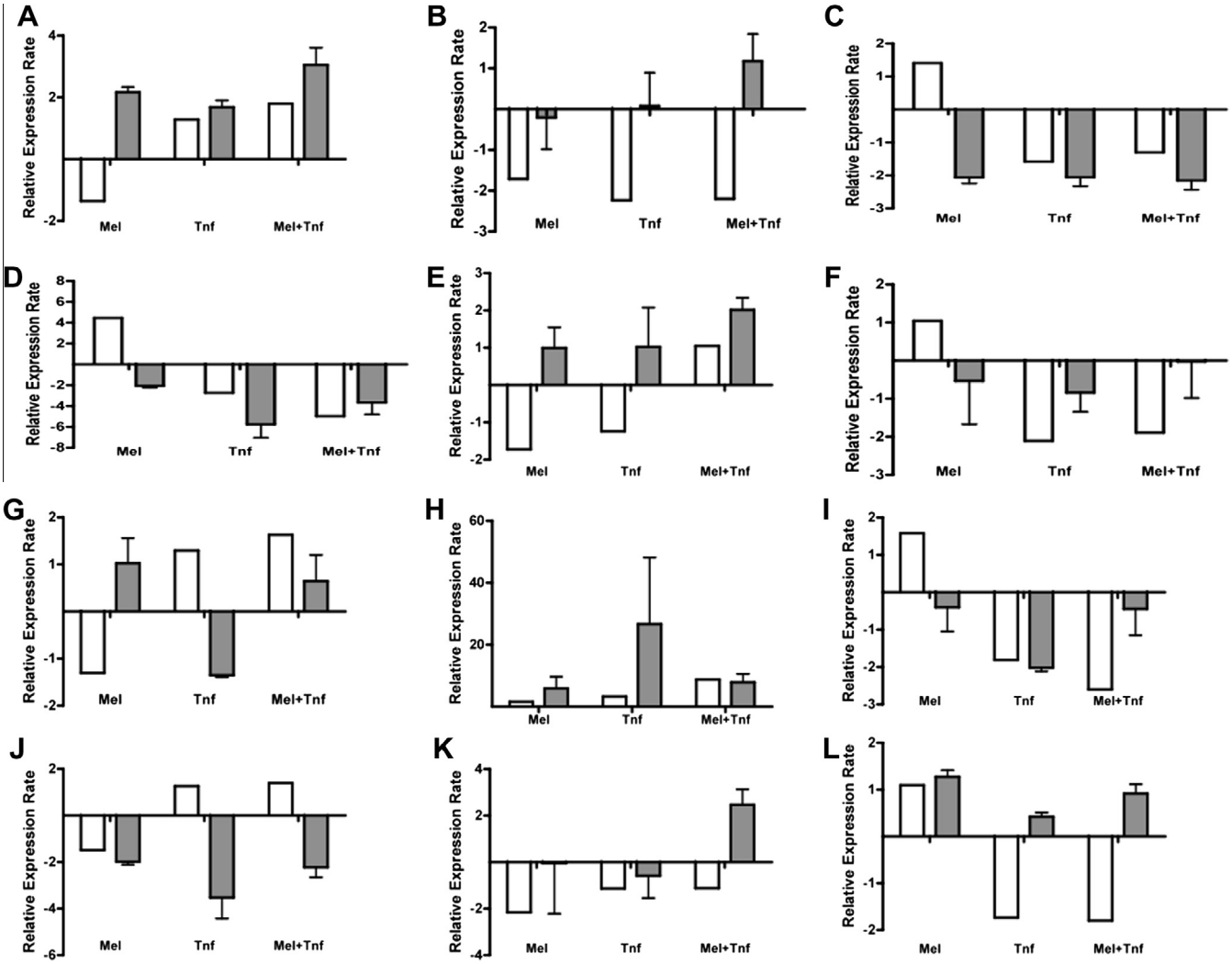

Fig. 4. Comparison between relative gene expression assessed by real time PCR and microarray. Boxes represent relative gene expression rate obtained with real time PCR (grey boxes) and microarray (white boxes) experiments. (A) *Bcl2l11*, (B) *Arhgef6*, (C) *Ptprj*, (D) *Fabp4*, (E) *Dlg5*, (F) *Cck*, (G) *Irak1bp1*, (H) *Ifi202b*, (I) *Flt1*, (J) *Palld*, (K) *Pard3*, (L) *Pecam1*.

late response observed in ILP patients treated with TNF-alpha and Mel. As FLT1 activation correlates with the inhibition of dendritic cell maturation and T cell proliferation, the release of dendritic cells from the suppressive effect of FLT1 may result in enhanced tumor antigen presentation and allow for a more efficient and long-lasting response against the tumor [42,43]. FLT1 production is associated with a worse prognosis in melanomas [44]. Patterson et al. [45] have demonstrated that TNF-alpha blocks VEGF-induced DNA synthesis in human endothelial cells and reduces FLT1 and KDR expression levels. Gille et al. [46] have observed, using a model employing B16 melanomas, that the full inhibition of tumor growth and lung metastasis is dependent on the inhibition of both FLT1 and KDR. Interestingly, blocking FLT1 significantly reduced CD45-positive inflammatory cell tumor infiltration. Therapies directed towards PLGF or FLT1 are also very attractive, as suggested by the work of Fischer et al. [47].

Fabp4 encodes FABP4, a small protein that binds to lipophilic compounds, forming complexes that interact in the nucleus with Pparg (peroxisome proliferator-activated receptor gamma), thereby taking part in adipocyte differentiation, glucose homeostasis, inflammation, and anti-proliferative activity against various carcinoma types [48]. Although *Fabp4* was not found to be differentially expressed in treated tumors compared with control tumors, we examined this gene further via real time PCR, as it presented the highest value of relative expression rates. Indeed, the *Fabp4* gene was downregulated in the groups treated with TNF-alpha. Reduced expression of FABP4 has been shown to correlate with a higher stage and histological grade in bladder cancer [49]. In contrast, *Fabp4* is induced by VEGFA and FGF2 and its knockdown abolishes the angiogenesis induced by these growth factors but not by FLT1 ligands [50]. PPARG is an interesting pharmacological target, as there is growing evidence that suggests a pro-apoptotic effect for some PPARG agonists [51] and a synergistic tumoricidal activity against melanoma when combined with bortezomib [32].

Most certainly, the additional differentially expressed genes also play a role in this model, and further studies are necessary to better understand their function in the context of our experimental model.

5. Conclusions

In this study, melphalan induced melanoma regression in a murine model when administered intravenously and was associated with mitotic inhibition and a prolongation of time to tumor progression. TNF-alpha promoted extensive necrosis in the tumors, but this was not associated with increased animal survival.

A set of 118 early expression genes was regulated in tumors by treatment with melphalan, TNF-alpha or a combination of the two

Table 2
Genes modulated by treatment with Mel, TNF-alpha, or both in melanoma. The genes listed here showed variations in their expression levels compared with controls. The complete list of differentially expressed genes is shown in the online Supplementary data (Table 3).

Comparison	Mel/control	Tnf/control	Mel + Tnf/control
Up-modulated genes	*Pdia6*, *Aff1*, *Oprm1*, *Efna3*, *Orc1l*, *Extl2*	*Ddx20*, *Polr1e*, *Cdc7*, *Pms2*	***Ifi202b***, ***Zc3hav1***, ***Igf2bp3***, *Neb*, *Atpbd4*, *Lepre1*, *Trp73*, *Trim24*, *Cdc7*, *Irak1bp1*, *Col4a3bp*, *Zfp622*, *4930544g21rik*, *Polr1e*, *Pou2f1*, *Camk2d*, *Btbd3*, *Efna3*, *Ubap1*, *Slc25a33*, *Tacc2*, *Rps6ka3*, *Ube4b*, *Trpc2*, *Igsf4a*, *Mphosph10*, *Tcfe3*
Down-modulated genes	***Crls1***, ***Pard3***, *Dlg5*, *Mib2*, *Kif1b*, *Orf61*, *Cdc37l1*, *Ltbp3*, *Mrp149*, *Mad1l1*, *Bc017158*, *Acbd6*, *Pms2*, *Col4a6*	***Arhgef6***, *Ptprj*, *Cck*, *Mrpl49*, *Cdc37l1*, *Ift122*, *Sdsl*	***Glul***, ***Arhgef6***, ***Aph1c***, ***Flt1***, ***Art5***, ***Cck***, *Pecam1*, *Rnf135*, *Kifap3*, *Napb*, *Glul*, *Tmem176b*, *Trpm1*, *Fbxw8*, *Tia1*, *Cdc37l1*, *Angel2*, *E2f1*, *Atp6v1c1*, *2310038h17rik*, *Rnf130*, *Cklf*, *Rbpms*, *Tmem176b*, *Ift122*, *Abhd12*, *Pcolce*, *Mgll*, *Bc033915*, *Pccb*, *Sdsl*, *Wbp1*, *Cpsf1*

Genes up-regulated when compared to control group are listed in the upper line and those down-regulated in the bottom line. All genes listed below had p value $\leqslant 0.05$ for the comparison against the control group and those with expression fold $\geqslant 2.0$ are highlighted in bold.

drugs, and a non-supervised hierarchical clusterization was capable of segregating the tumors submitted to each of the aforementioned treatments.

Although our data display some limitations that are inherent to the experimental model adopted, the results provide insight into very interesting potential therapeutic strategies that could reproduce systemically, with lower toxicity, some of the synergistic effects of TNF-alpha and Mel that have been observed in ILP. Based on these results, experiments using mixed co-cultures of melanoma, macrophages and endothelial cells are ongoing for functional validation. Treatment with a combination of drugs that target some of the proteins encoded by the genes discussed in this report may be utilized to both improve the overall antitumoral effect of each isolated compound and minimize toxicity.

Acknowledgements

This work was funded by the State of São Paulo Research Foundation (FAPESP). We thank all members of our laboratory for helpful discussions, Dr. Elaine Rodrigues from UNIFESP for providing the B16F10 cells, the São Paulo branch of the Ludwig Institute for Cancer Research for providing the B16F1 cells, Carlos Ferreira Nascimento and Suely Nonogaki for technical assistance, as well as Wanderley Lourenço Gonçalves, Oraci de Lima Leite, and Ederval de Oliveira Machado for animal care.

Appendix A. Supplementary material

Supplementary data associated with this article can be found, in the online version, at http://dx.doi.org/10.1016/j.cyto.2013.02.022.

References

[1] Miller AJ, Mihm Jr MC. Melanoma. N Engl J Med 2006;355:51–65.
[2] Tsao H, Atkins MB, Sober AJ. Management of cutaneous melanoma. N Engl J Med 2004;351:998–1012.
[3] Balch CM, Gershenwald JE, Soong SJ, Thompson JF, Atkins MB, Byrd DR, et al. Final version of 2009 AJCC melanoma staging and classification. J Clin Oncol 2009.
[4] Wheatley K, Ives N, Hancock B, Gore M, Eggermont A, Suciu S. Does adjuvant interferon-alpha for high-risk melanoma provide a worthwhile benefit? A meta-analysis of the randomised trials. Cancer Treat Rev 2003;29:241–52.
[5] Cornett WR, McCall LM, Petersen RP, Ross MI, Briele HA, Noyes RD, et al. Randomized multicenter trial of hyperthermic isolated limb perfusion with melphalan alone compared with melphalan plus tumor necrosis factor: American College of Surgeons Oncology Group Trial Z0020. J Clin Oncol 2006;24:4196–201.
[6] Rossi CR, Foletto M, Pilati P, Mocellin S, Lise M. Isolated limb perfusion in locally advanced cutaneous melanoma. Semin Oncol 2002;29:400–9.
[7] Grunhagen DJ, de Wilt JH, van Geel AN, Eggermont AM. Isolated limb perfusion for melanoma patients – a review of its indications and the role of tumor necrosis factor-alpha. Eur J Surg Oncol 2006;32:371–80.
[8] Bauer GB, Povirk LF. Specificity and kinetics of interstrand and intrastrand bifunctional alkylation by nitrogen mustards at a G-G-C sequence. Nucleic Acids Res 1997;25:1211–8.
[9] Lienard D, Eggermont AM, Koops HS, Kroon B, Towse G, Hiemstra S, et al. Isolated limb perfusion with tumor necrosis factor-alpha and melphalan with or without interferon-gamma for the treatment of in-transit melanoma metastases: a multicenter randomized phase II study. Melanoma Res 1999;9:491–502.
[10] Noorda EM, Vrouenraets BC, Nieweg OE, van Geel BN, Eggermont AM, Kroon BB. Isolated limb perfusion for unresectable melanoma of the extremities. Arch Surg 2004;139:1237–42.
[11] Hayes AJ, Neuhaus SJ, Clark MA, Thomas JM. Isolated limb perfusion with melphalan and tumor necrosis factor alpha for advanced melanoma and soft-tissue sarcoma. Ann Surg Oncol 2007;14:230–8.
[12] de Wilt JH, ten Hagen TL, de BG, van Tiel ST, de Bruijn EA, Eggermont AM. Tumor necrosis factor alpha increases melphalan concentration in tumor tissue after isolated limb perfusion. Br J Cancer 2000;82:1000–3.
[13] Lejeune FJ, Lienard D, Matter M, Ruegg C. Efficiency of recombinant human TNF in human cancer therapy. Cancer Immunol 2006;6:6.
[14] Renard N, Lienard D, Lespagnard L, Eggermont A, Heimann R, Lejeune F. Early endothelium activation and polymorphonuclear cell invasion precede specific necrosis of human melanoma and sarcoma treated by intravascular high-dose tumor necrosis factor alpha (rTNF alpha). Int J Cancer 1994;57:656–63.
[15] Ruegg C, Yilmaz A, Bieler G, Bamat J, Chaubert P, Lejeune FJ. Evidence for the involvement of endothelial cell integrin alphaVbeta3 in the disruption of the tumor vasculature induced by TNF and IFN-gamma. Nat Med 1998;4:408–14.
[16] Stoelcker B, Ruhland B, Hehlgans T, Bluethmann H, Luther T, Mannel DN. Tumor necrosis factor induces tumor necrosis via tumor necrosis factor receptor type 1-expressing endothelial cells of the tumor vasculature. Am J Pathol 2000;156:1171–6.
[17] Gomes LI, Silva RL, Stolf BS, Cristo EB, Hirata R, Soares FA, et al. Comparative analysis of amplified and nonamplified RNA for hybridization in cDNA microarray. Anal Biochem 2003;321:244–51.
[18] Saeed AI, Sharov V, White J, Li J, Liang W, Bhagabati N, et al. TM4: a free, open-source system for microarray data management and analysis. Biotechniques 2003;34:374–8.
[19] Pfaffl MW. A new mathematical model for relative quantification in real-time RT–PCR. Nucleic Acids Res 2001;29:e45.
[20] Moreno-Ramirez D, Cruz-Merino L, Ferrandiz L, Villegas-Portero R, Nieto-Garcia A. Isolated limb perfusion for malignant melanoma: systematic review on effectiveness and safety. Oncologist 2010;15:416–27.
[21] Asher A, Mule JJ, Reichert CM, Shiloni E, Rosenberg SA. Studies on the anti-tumor efficacy of systemically administered recombinant tumor necrosis factor against several murine tumors *in vivo*. J Immunol 1987;138:963–74.
[22] Perona R, Montaner S, Saniger L, Sanchez-Perez I, Bravo R, Lacal JC. Activation of the nuclear factor-kappaB by Rho, CDC42, and Rac-1 proteins. Genes Dev 1997;11:463–75.
[23] Bialkowska K, Kulkarni S, Du X, Goll DE, Saido TC, Fox JE. Evidence that beta3 integrin-induced Rac activation involves the calpain-dependent formation of integrin clusters that are distinct from the focal complexes and focal adhesions that form as Rac and RhoA become active. J Cell Biol 2000;151:685–96.
[24] Filipenko NR, Attwell S, Roskelley C, Dedhar S. Integrin-linked kinase activity regulates Rac- and Cdc42-mediated actin cytoskeleton reorganization via alpha-PIX. Oncogene 2005;24:5837–49.
[25] Rosenberger G, Kutsche K. AlphaPIX and betaPIX and their role in focal adhesion formation. Eur J Cell Biol 2006;85:265–74.
[26] Rosenberger G, Jantke I, Gal A, Kutsche K. Interaction of alphaPIX (ARHGEF6) with beta-parvin (PARVB) suggests an involvement of alphaPIX in integrin-mediated signaling. Hum Mol Genet 2003;12:155–67.
[27] Deshpande SS, Angkeow P, Huang J, Ozaki M, Irani K. Rac1 inhibits TNF-alpha-induced endothelial cell apoptosis: dual regulation by reactive oxygen species. FASEB J 2000;14:1705–14.

[28] Porchia LM, Guerra M, Wang YC, Zhang Y, Espinosa AV, Shinohara M, et al. 2-amino-N-{4-[5-(2-phenanthrenyl)-3-(trifluoromethyl)-1H-pyrazol-1-yl]-phenyl} acetamide (OSU-03012), a celecoxib derivative, directly targets p21-activated kinase. Mol Pharmacol 2007;72:1124–31.
[29] Fang L, Wang Y, Du D, Yang G, Tak KT, Kai KS, et al. Cell polarity protein Par3 complexes with DNA-PK via Ku70 and regulates DNA double-strand break repair. Cell Res 2007;17:100–16.
[30] Ma XY, Wang H, Ding B, Zhong H, Ghosh S, Lengyel P. The interferon-inducible p202a protein modulates NF-kappaB activity by inhibiting the binding to DNA of p50/p65 heterodimers and p65 homodimers while enhancing the binding of p50 homodimers. J Biol Chem 2003;278:23008–19.
[31] Wen Y, Yan DH, Wang B, Spohn B, Ding Y, Shao R, et al. P202, an interferon-inducible protein, mediates multiple antitumor activities in human pancreatic cancer xenograft models. Cancer Res 2001;61:7142–7.
[32] Freudlsperger C, Thies A, Pfuller U, Schumacher U. The proteasome inhibitor bortezomib augments anti-proliferative effects of mistletoe lectin-I and the PPAR-gamma agonist rosiglitazone in human melanoma cells. Anticancer Res 2007;27:207–13.
[33] Jiang Z, Chu PG, Woda BA, Rock KL, Liu Q, Hsieh CC, et al. Analysis of RNA-binding protein IMP3 to predict metastasis and prognosis of renal-cell carcinoma: a retrospective study. Lancet Oncol 2006;7:556–64.
[34] Pryor JG, Bourne PA, Yang Q, Spaulding BO, Scott GA, Xu H. IMP-3 is a novel progression marker in malignant melanoma. Mod Pathol 2008;21:431–7.
[35] Mentrikoski MJ, Ma L, Pryor JG, McMahon LA, Yang Q, Spaulding BO, et al. Diagnostic utility of IMP3 in segregating metastatic melanoma from benign nevi in lymph nodes. Mod Pathol 2009;22:1582–7.
[36] Mathieu V, Mijatovic T, Van DM, Kiss R. Gastrin exerts pleiotropic effects on human melanoma cell biology. Neoplasia 2005;7:930–43.
[37] Chang AJ, Song DH, Wolfe MM. Attenuation of peroxisome proliferator-activated receptor gamma (PPARgamma) mediates gastrin-stimulated colorectal cancer cell proliferation. J Biol Chem 2006;281:14700–10.
[38] Carrillo J, Garcia-Aragoncillo E, Azorin D, Agra N, Sastre A, Gonzalez-Mediero I, et al. Cholecystokinin down-regulation by RNA interference impairs Ewing tumor growth. Clin Cancer Res 2007;13:2429–40.
[39] Takenaka K, Katakura H, Chen F, Ogawa E, Adachi M, Wada H, et al. The ratio of membrane-bound form Flt-1 mRNA to VEGF mRNA correlates with tumor angiogenesis and prognosis in non-small cell lung cancer. Cancer Lett 2007;246:34–40.
[40] Kerber M, Reiss Y, Wickersheim A, Jugold M, Kiessling F, Heil M, et al. Flt-1 signaling in macrophages promotes glioma growth *in vivo*. Cancer Res 2008;68:7342–51.
[41] Hiratsuka S, Maru Y, Okada A, Seiki M, Noda T, Shibuya M. Involvement of Flt-1 tyrosine kinase (vascular endothelial growth factor receptor-1) in pathological angiogenesis. Cancer Res 2001;61:1207–13.
[42] Dikov MM, Ohm JE, Ray N, Tchekneva EE, Burlison J, Moghanaki D, et al. Differential roles of vascular endothelial growth factor receptors 1 and 2 in dendritic cell differentiation. J Immunol 2005;174:215–22.
[43] Lin YL, Liang YC, Chiang BL. Placental growth factor down-regulates type 1 T helper immune response by modulating the function of dendritic cells. J Leukocyte Biol 2007;82:1473–80.
[44] Straume O, Akslen LA. Expresson of vascular endothelial growth factor, its receptors (FLT-1, KDR) and TSP-1 related to microvessel density and patient outcome in vertical growth phase melanomas. Am J Pathol 2001;159:223–35.
[45] Patterson C, Perrella MA, Endege WO, Yoshizumi M, Lee ME, Haber E. Downregulation of vascular endothelial growth factor receptors by tumor necrosis factor-alpha in cultured human vascular endothelial cells. J Clin Invest 1996;98:490–6.
[46] Gille J, Heidenreich R, Pinter A, Schmitz J, Boehme B, Hicklin DJ, et al. Simultaneous blockade of VEGFR-1 and VEGFR-2 activation is necessary to efficiently inhibit experimental melanoma growth and metastasis formation. Int J Cancer 2007;120:1899–908.
[47] Fischer C, Jonckx B, Mazzone M, Zacchigna S, Loges S, Pattarini L, et al. Anti-PlGF inhibits growth of VEGF(R)-inhibitor-resistant tumors without affecting healthy vessels. Cell 2007;131:463–75.
[48] Ayers SD, Nedrow KL, Gillilan RE, Noy N. Continuous nucleocytoplasmic shuttling underlies transcriptional activation of PPARgamma by FABP4. Biochemistry 2007;46:6744–52.
[49] Boiteux G, Lascombe I, Roche E, Plissonnier ML, Clairotte A, Bittard H, et al. A-FABP, a candidate progression marker of human transitional cell carcinoma of the bladder, is differentially regulated by PPAR in urothelial cancer cells. Int J Cancer 2009;124:1820–8.
[50] Elmasri H, Karaaslan C, Teper Y, Ghelfi E, Weng M, Ince TA, et al. Fatty acid binding protein 4 is a target of VEGF and a regulator of cell proliferation in endothelial cells. FASEB J 2009;23:3865–73.
[51] Panigrahy D, Huang S, Kieran MW, Kaipainen A. PPARgamma as a therapeutic target for tumor angiogenesis and metastasis. Cancer Biol Ther 2005;4:687–93.